Available online at www.sciencedirect.com
ScienceDirect
Wear 263 (2007) 258–264
WEAR
www.elsevier.com/locate/wear

Case study

Slurry erosion of thermal spray coatings and stainless steels for hydraulic machinery

J.F. Santa, J.C. Baena, A. Toro *

Tribology and Surfaces Group, National University of Colombia, Medellín, Colombia

Received 2 September 2006; received in revised form 30 November 2006; accepted 3 December 2006
Available online 23 May 2007

Abstract

The slurry erosion of two coatings applied by oxy fuel powder (OFP) and wire arc spraying (WAS) processes onto sand-blasted AISI 304 steel was studied, and the results were compared to those obtained with AISI 431 and ASTM A743 grade CA6NM stainless steels, which are commonly used for hydraulic turbines and accessories. The adherence of the coatings to the substrate was measured according to ASTM C 633 standard, while the microstructure and worn surfaces were characterized by optical and scanning electron microscopy. Slurry erosion tests were carried out in a modified centrifugal pump, in which the samples were placed conveniently to ensure grazing incidence of the particles. The slurry was composed of distilled water and quartz sand particles with an average diameter between 212 and 300 μm (AFS 50/70) and the solids content was 10 wt% in all the tests. The mean impact velocity of the slurry was 5.5 m/s and the erosion resistance was determined from the volume loss results. The coated surfaces showed higher erosion resistance than the uncoated stainless steels, with the lower volume losses measured for the E-C 29123 deposit. SEM analysis of the worn surfaces revealed intense plastic deformation in both coated and bare stainless steels, with little evidence of brittle fracture in the microstructure. The measured adhesive strength of the coatings was considered acceptable for the processes employed.

Keywords: Slurry erosion; Microstructure; Thermal spray coatings; Hydraulic turbines

1. Introduction

Stainless steels are widely used in hydroelectric power plants due to their good corrosion properties and acceptable resistance to solid particle erosion, since many components are in contact with aqueous solutions containing hard particles that impact against the surface causing significant material loss (slurry erosion condition). The magnitude of the damage caused is a consequence of the amount, type and size of solid particles in the flow, together with the mechanical properties of the surfaces, physical–chemical properties of the water and operating conditions [1,2].

Slurry erosion problems are particularly important during rainy seasons due to the increase in the number of solid particles impacting the surfaces, especially in systems where an exhaustive filtration process is not possible. This is the case of the Francis turbines installed in a hydroelectric power plant in northwestern Colombia, where intense erosive wear has led to changes in surface texture and loss of adjustment between the liners and the spiral case, as can be seen in Fig. 1.

The angle of incidence of the particles is extremely important to determine the main wear mechanism acting on the surface of the components submitted to erosion. It is well known that micro-cutting prevails for low impact angles whereas for angles close to 90° the dominant effects are low-cycle fatigue and accumulation of plastic deformation up to a critical value that promotes material detaching [3,4]. In addition, corrosive attack and boundary layer effects develop when the particles are carried by a liquid, configuring a much more intricate situation that is affected by the rheological properties of the carrying fluid such as its density and viscosity [5,6].

A cost-effective way to improve the slurry erosion resistance of the components is the application of thermally sprayed coatings [7,8]. The term thermal spray describes a family of processes that use chemical or electrical energy to melt (or soften) and accelerate particles of a material which is then deposited on a surface [9]. The coatings may have a good erosion resistance depending on the chemical and mechanical properties of the material deposited, the surface preparation prior to application and the deposition conditions [7–9].

* Corresponding author. Tel.: +57 4 425 5339; fax: +57 4 425 5339.
E-mail address: aotoro@unal.edu.co (A. Toro).

0043-1648/$ – see front matter © 2007 Elsevier B.V. All rights reserved.
doi:10.1016/j.wear.2006.12.061

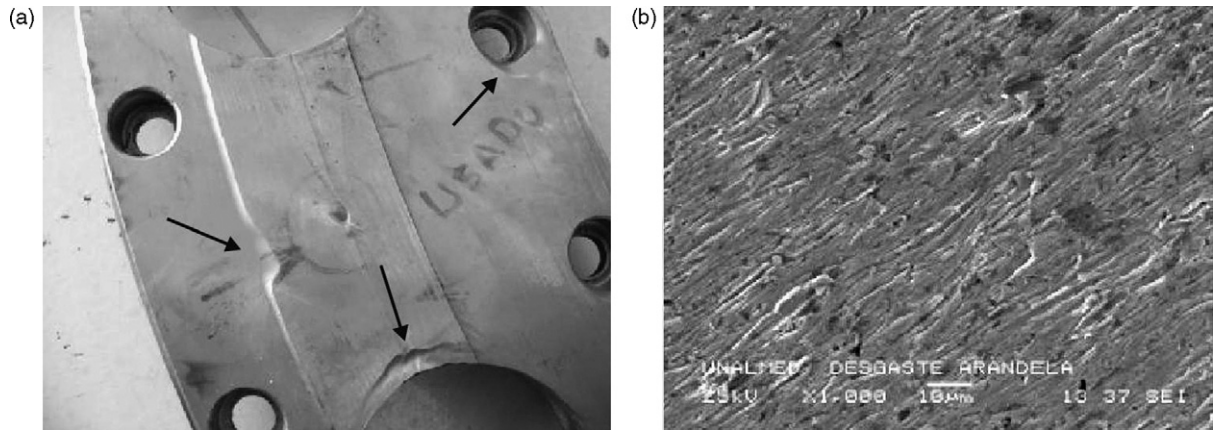

Fig. 1. Liner of a Francis turbine. (a) General aspect of liner's worn surface and (b) detailed view showing wear marks (SEM). Arrows in (a) indicate preferential locals for erosive wear.

In this work, two thermally sprayed coatings were studied in laboratory in order to evaluate their potential application in a particular component of a Francis hydraulic turbine. The evaluation included the analysis of the worn component and comparison between coated and uncoated samples submitted to controlled slurry erosion conditions.

2. Experimental procedure

2.1. Materials

Two stainless steels commonly used for turbines and hydraulic accessories were used, namely ASTM A743—grades CA6NM and AISI 431, whose nominal chemical compositions are shown in Table 1. Also, two commercial powders, E-C 29123 (WC/Co in Fe–Cr–Ni matrix) and T 35MXC (Al_2O_3-reinforced high-carbon steel) were deposited onto AISI 304 steel by oxy-fuel powder (OFP) and wire arc spraying (WAS) processes, respectively. The coatings were deposited by using Terodyn 2000 (OFP process) and TAFA 8830 (WAS process) equipments according to the manufacturers recommendations. The surfaces were prepared either by sand blasting (OFP coatings) or grinding wheel (WAS coatings). In all cases a nickel-rich bond-pass was applied before the wear-resistant coating.

2.2. Microstructure and chemical characterization

The microstructure characterization was done in a JEOL 5910LV SEM and an Olympus PME3 LOM. The porosity of the coatings was measured by digital image analysis. Vickers hardness and micro-hardness measurements were performed by using a Wolpert hardness tester ($HV_{62.5\,kgf}$) and a Shimadzu micro-hardness tester ($HV_{300\,g,\,15\,s}$), respectively. Localized chemical analyses of the specimens were done with an EDS spectrometer coupled to the SEM. The AISI 431 stainless steel samples were taken from the liner of a Francis turbine that presented accelerated wear damage, while the specimens of ASTM A743 grade CA6NM stainless steel and the coatings were prepared in laboratory.

2.3. Slurry erosion tests

The slurry erosion tests were carried out in a modified centrifugal pump, in which the specimens were submitted to wear conditions similar to those of the liners of Francis hydraulic turbines. Fig. 2 shows the configuration of the testing machine, which is composed of a commercial centrifugal pump connected to an electrical motor, a frequency inverter and an isothermal bath to control the slurry temperature. The samples were located at the outlet of the centrifugal pump to ensure grazing incidence of the particles (see Fig. 2). The slurry was composed of distilled water and quartz particles with a mean diameter between 212 and 300 μm (AFS 50/70) and the solids content was 10 wt%. The mean impact velocity of the slurry was 5.5 m/s and the erosion resistance was determined from the mass loss results. Mass losses were measured every 30 min by using a scale with 0.01 mg resolution. The total duration of each test was 120 min, and after that period both the sample and the slurry were replaced.

2.4. Analysis of worn surfaces

The worn surfaces were analyzed in stereoscopic and scanning electron microscopes in order to identify the wear mechanisms and relate them to the mass loss results.

Table 1
Nominal chemical composition of the studied stainless steels (wt%)

Material	C	Mn	Si	Cr	Ni	P	S	Mo	Others
AISI 431	0.20	1.00	1.00	15.0–17.0	1.25–2.50	0.04	0.03	–	Fe balance
ASTM A743—grade CA6NM	0.06	Max. 1	Max. 1	11.5–14	3.5–4.5	Max. 0.04	Max. 0.03	0.4–1.0	Fe balance
E-C 29123	–	–	–	3–7	15–40	–	–	–	W >60, Co 7–13
35 MXC	Steel tube filled with Al-rich particles								

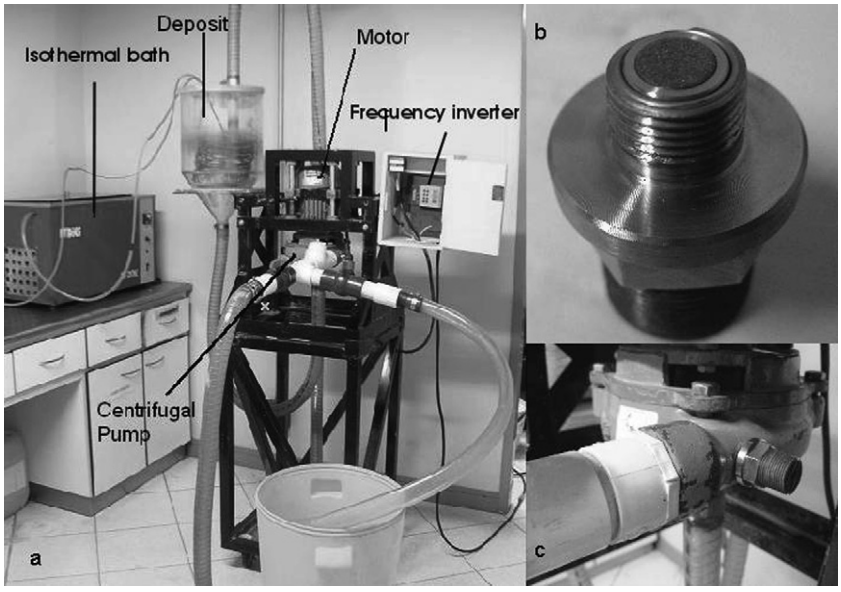

Fig. 2. Slurry erosion testing machine. (a) General aspect of the device, (b) detail of sample-holder and (c) detail of positioning of the samples in the centrifugal pump.

3. Results and discussion

3.1. Microstructure

3.1.1. AISI 431 stainless steel

The microstructure of this steel is composed of martensite with chromium carbides precipitated at the prior austenite grain boundaries, as can be seen in Fig. 3. The average hardness measured was 320 $HV_{62.5\,kg\,f}$. Micro-hardness measurements reported 422 $HV_{25\,g\,f,\,15\,s}$. in the martensitic matrix.

3.1.2. ASTM A743 grade CA6NM stainless steel

The material received in the as-cast condition was homogenized at 1050 °C for 1 h and then air-cooled to room temperature. After that, the specimens were tempered at 650 °C for 1 h and cooled down in air. The microstructure of the steel is composed of martensite (average hardness 280 $HV_{62.5\,kg\,f}$) with some retained austenite and δ-ferrite (Fig. 4). Micro-hardness measurements of martensite reported 367 $HV_{25\,g\,f,\,15\,s.}$

3.1.3. E-C 29123 coating

Fig. 5 shows the microstructure of a typical coating with a thickness of circa 400 μm including the bonding layer of 100 μm. The bonding layer is composed by a soft, nickel-rich matrix (191 HV average hardness) containing elongated aluminum oxide particles (1530 $HV_{25\,g\,f,\,15\,s}$), which are marked as (1) in Fig. 5. The measured average volume fractions of Al_2O_3 particles and pores were 11% and 7%, respectively. The wear-resistant E-C 29123 coating is composed of hard, WC/Co particles (1211 HV average hardness) and softer Ni–Cr regions (639 HV average hardness), together with a number of unmelted particles and pores. The volume fraction of pores was estimated

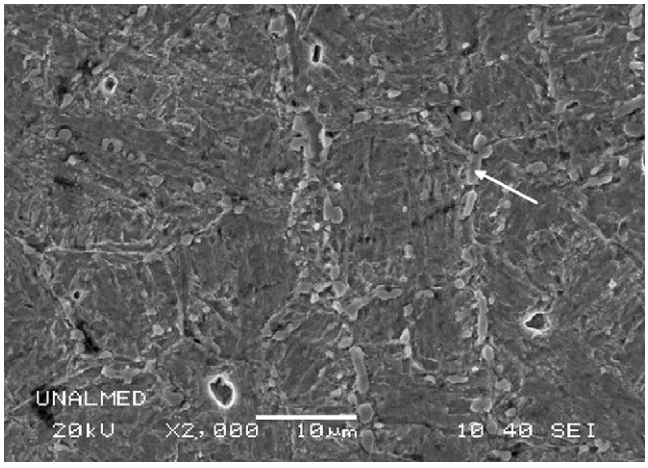

Fig. 3. Microstructure of AISI 431 stainless steel, Kalling's 2, 2000×, SEM. The arrow shows a chromium carbide precipitated at the grain boundary of prior austenite.

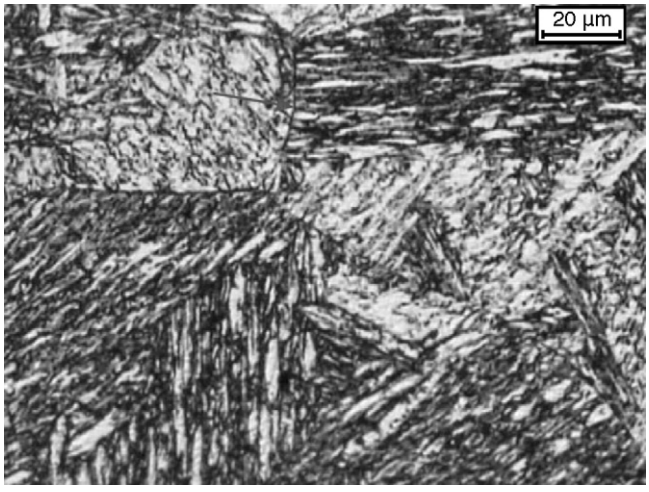

Fig. 4. Microstructure of ASTM A743 CA6NM stainless steel, Vilella's, 860×. LOM.

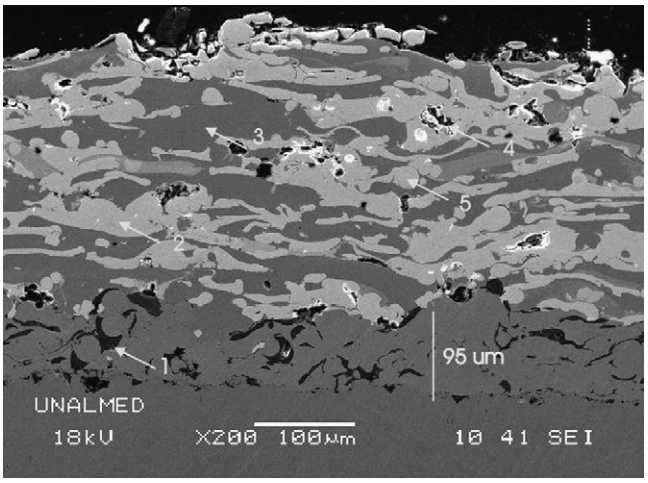

Fig. 5. Microstructure of E-C 29123 coating, 200×, SEM. (1) Aluminum oxide, (2) WC particles, (3) Ni–Fe–Cr particle, (4) porosity and (5) unmelted particle.

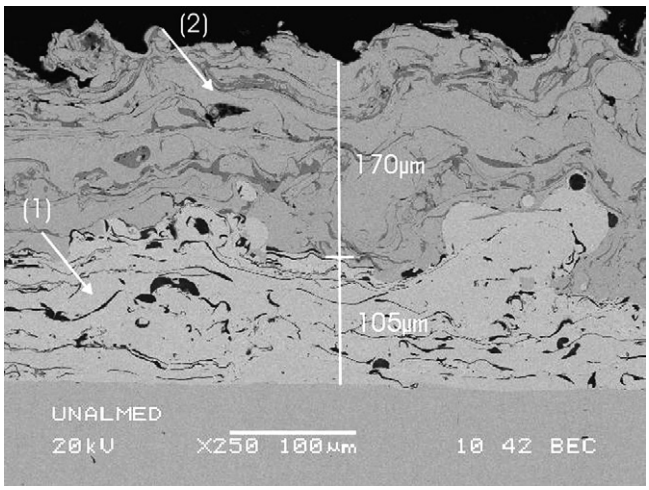

Fig. 6. Microstructure of T 35 MXC coating, 300×, SEM. (1) Aluminum oxide in bond pass and (2) pore in wear-resistant layer.

to 15% by digital image processing of SEM images. This porosity amount is acceptable for OFP coatings [10]. The ASTM C633 tests reported a mean adhesive strength of 7.9 MPa with total detachment of the bond pass. This average value is in agreement with literature for the OFP process [9,10] and it is an indication of acceptable quality of the coatings.

3.1.4. T 35 MXC coating

The microstructure of T 35 MXC coating can be seen in Fig. 6. The thickness of the coating was circa 270 μm including the bonding layer of 100 μm. The bonding layer is composed of a Ni-rich matrix containing a volume fraction of 10% of elongated aluminum oxides (2100 $HV_{200\,g,\,15\,s}$) and average porosity of 4%. The microstructure of the wear-resistant coating T 35 MXC (238 $HV_{300\,g,\,15\,s}$) is a distribution of aluminum oxides in a high carbon steel matrix. The measured volume fraction of aluminum oxides and porosity were 12% and 15%, respectively.

3.2. Examination of worn surfaces

The typical aspect of the worn surfaces as seen in stereographic microscope is shown in Fig. 7. Detailed analysis of the worn surfaces revealed wear marks typical of erosion at grazing incidence, with micro-cutting and micro-ploughing as the main wear mechanisms observed at the surface of all the stainless steels tested and the T 35 MXC coating (Fig. 8), being these marks more evident and evenly distributed in the stainless steel samples. On the other hand, the worn surfaces of the E-C 29123 coatings showed a differential response as a function of the phases present in the microstructure, as shown in Fig. 9.

Aluminum oxides in T 35 MXC and WC/Co areas in E-C 29123 coatings contributed to increase the wear resistance due to their high hardness and Young modulus. As the testing time increased the hard phases were gradually exposed to the erosive particles and the main wear mechanism changed from micro-cutting of matrix to spalling of hard phases.

Evidences of brittle fracture were observed in the E-C 29123 coating, as can be seen in Fig. 9 (arrow in left upper corner). Nevertheless, the analysis of the coatings before the slurry erosion tests reveals that similar cracks are formed as a consequence of the thermal spray process employed, due to the high cooling speeds and the thermal coefficient mismatch between WC/Co particles and Ni–Cr regions (Fig. 10). Unmelted particles and droplets can also be observed before the surface is submitted to the slurry wear tests, but these features are removed during the tests due to their low adherence to the substrate.

A significant increase in micro-hardness was observed in the stainless steels surfaces after the slurry erosion tests, probably as a consequence of both martensitic transformation of retained austenite and work hardening effect. The measured average increase was 71 $HV_{25\,g\,f,\,15\,s}$ in AISI 431 steel and 114 $HV_{25\,g\,f,\,15\,s}$ in ASTM A743 grade CA6NM steel.

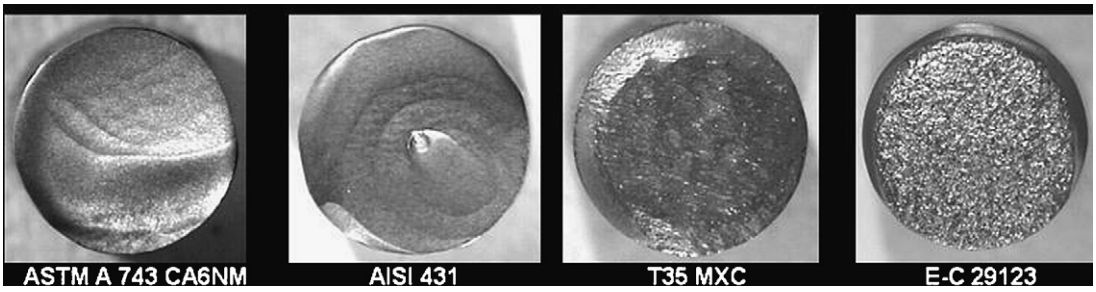

Fig. 7. Typical worn surfaces after slurry erosion tests, 10×, LOM.

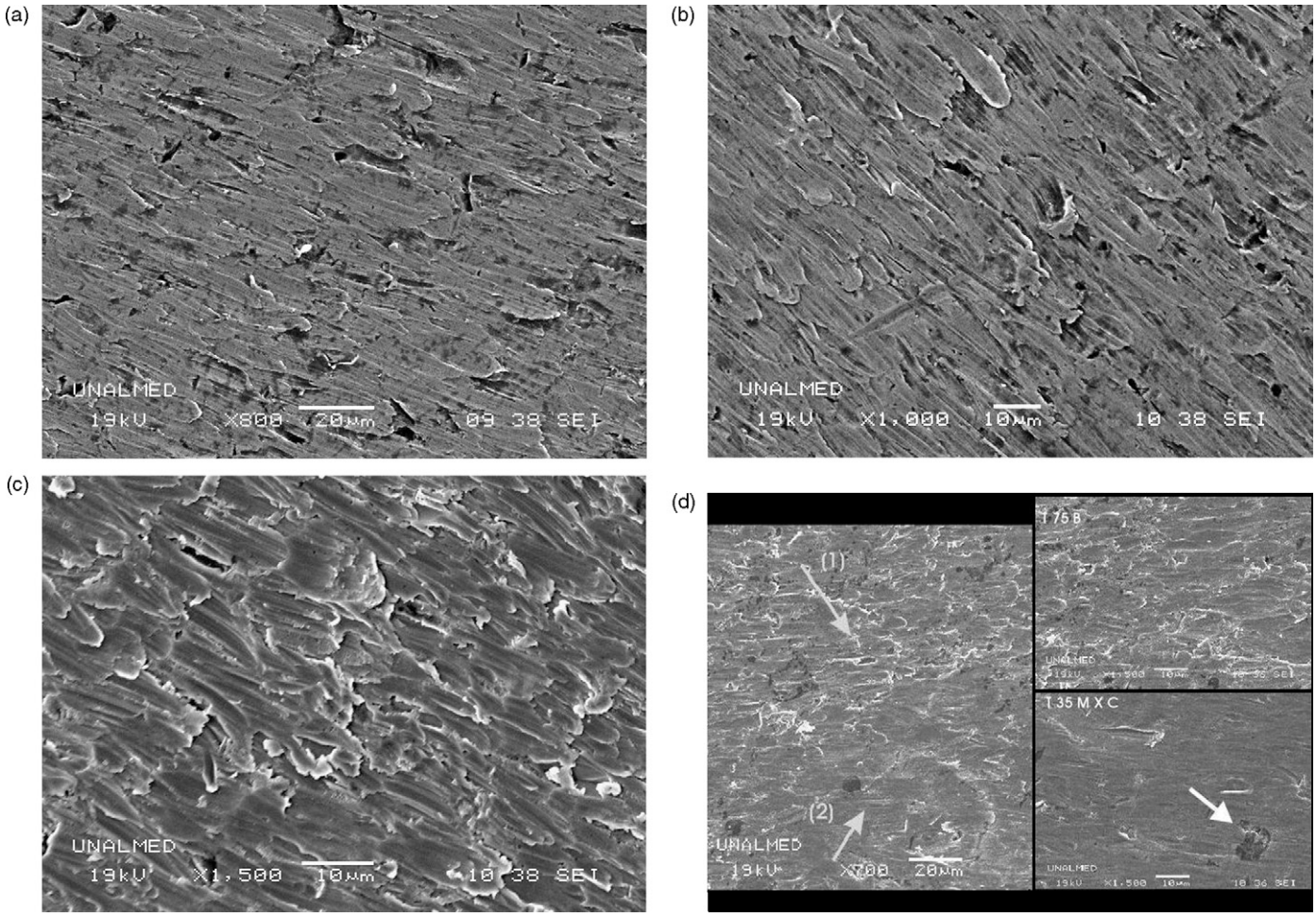

Fig. 8. SEM examination of worn surfaces. (a) AISI 431 stainless steel, (b) ASTM A743 CA6NM stainless steel, (c) AISI 304 stainless steel and (d) T 35 MXC coating.

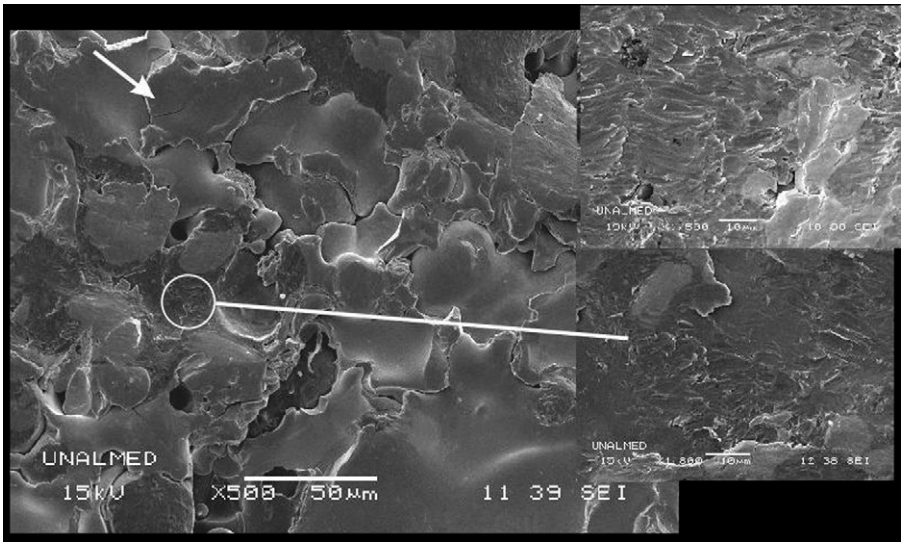

Fig. 9. SEM examination of the worn surface of E-C 29123 coating. Micro-cutting marks cover the soft areas while the harder phases are smooth.

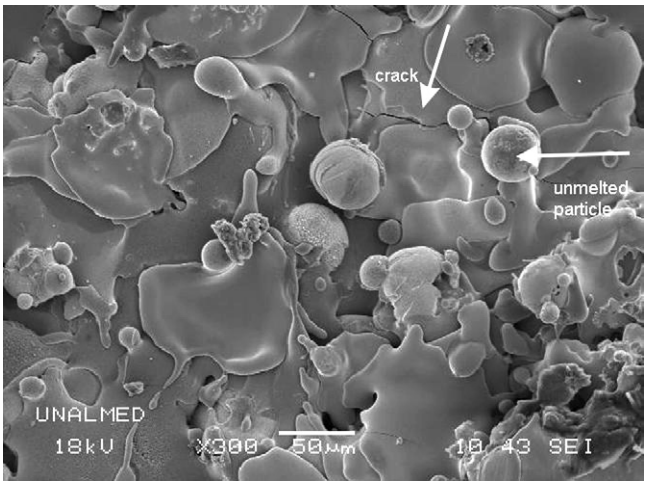

Fig. 10. Surface of E-C 29123 coating before the slurry erosion tests. Unmelted particles, droplets and cracks are shown.

3.3. Degradation of abrasive particles

The typical morphology of abrasive particles before the tests and the change in size distribution as a consequence of the erosive process are presented in Fig. 11. Note that after the tests the distribution is shifted to smaller grain sizes, which reveals fragmentation of the particles and subsequent loss of their ability to erode the surface of the samples.

3.4. Volume loss

The volume loss of all the samples in the slurry erosion tests is shown in Fig. 12. The reported values were calculated from the measured mass losses and average density values of each of the materials studied, namely 15.4 g/cm^3 for E-C coating, 6.35 g/cm^3 for T 35 MXC coating, and 7.7 g/cm^3 for AISI 431 and ASTM A743 grade CA6NM steels. The reported values of volume loss are the average of three tests performed under the same conditions.

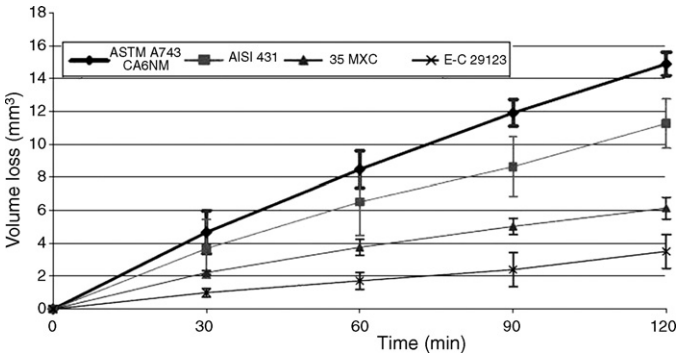

Fig. 12. Accumulate volume loss after slurry erosion tests.

Generally speaking, the uncoated stainless steels reported higher volume losses than the thermal sprayed coatings. The E-C 29123 coating showed the best erosion resistance, while the ASTM A743 grade CA6NM steel reported the highest mass losses of the tested materials.

It is worth noticing that the two uncoated stainless steels presented similar volume losses during the first stages of the tests (see error bars in Fig. 12). Nevertheless, after 90 min testing the AISI 431 samples undoubtedly showed better erosion resistance than ASTM A743 grade CA6NM samples, probably due to the differences in microstructure such as the presence of hard chromium carbides precipitated at grain boundaries.

4. Conclusions

- The E-C 29123 coating applied by OFP process onto AISI 304 stainless steel reported the best slurry erosion resistance of the studied materials, mainly as a consequence of the combined properties of hard, wear-resistant particles and a ductile metallic matrix.
- The studied coatings showed ability to deform plastically when submitted to slurry erosion conditions, with little evidence of mass removal by brittle fracture mechanisms. Unmelted particles and droplets are easily removed from the

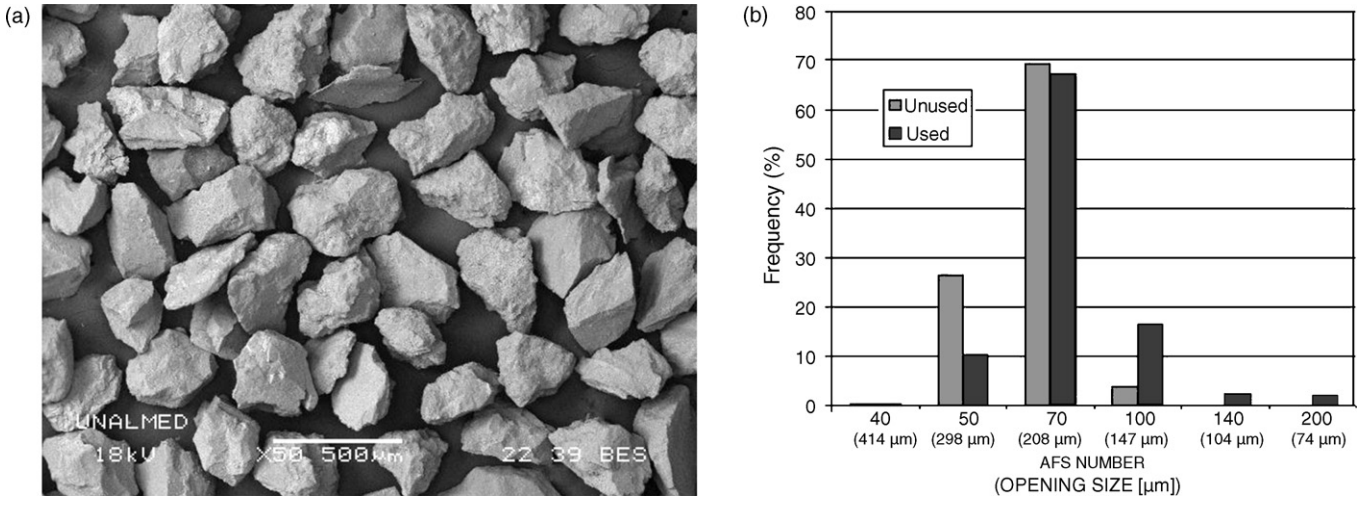

Fig. 11. (a) Morphology of quartz sand particles used in the tests and (b) grain size distribution before and after the tests (AFS number and opening size in micrometers).

surface, but this does not affect the overall performance of the coatings in terms of volume loss and main wear mechanisms.
- The applied coatings are an interesting alternative to enhance the wear resistance of components used in hydraulic machines, in particular under grazing incidence conditions and moderate-to-low mean impact velocities.

Acknowledgments

The authors thank to Empresas Públicas de Medellín E.S.P. and Metalizar S.A. for their technical support. Financial support provided by Colciencias-EPM-UNAL project no. 20201005975 is also acknowledged.

References

[1] J. Hengyun, et al., The role of sand particles on the rapid destruction of the cavitation zone of hydraulic turbines, Wear 112 (1986) 199–205.
[2] T.H. Kosel, Solid particle erosion, in: ASM Handbook, vol. 18, Friction, Lubrication and Wear Technology, ASM International, 1992, pp. 199–210.
[3] I.M. Hutchings, Tribology: Friction and Wear of Engineering Materials, Edward Arnold, Cambridge, 1992.
[4] K.H. Zum Gahr, Microstructure and Wear of Materials, Elsevier, Amsterdam, 1987.
[5] G. Sundararajan, A comprehensive model for the solid particle erosion of ductile materials, Wear 149 (1995) 111–127.
[6] A.V. Levy, P. Yau, Erosion of steels in liquid slurries, Wear 98 (1984) 163–182.
[7] K. Sugiyama, et al., Slurry wear and cavitation erosion of thermal-sprayed cermets, Wear 258 (2005) 768–775.
[8] P. Kulu, I. Hussainova, R. Veinthal, Solid particle erosion of thermal sprayed coatings, Wear 258 (2005) 488–496.
[9] D. Crawner, Thermal spray processes, in: Handbook of Thermal Spray Technologies, ASM International, 2004.
[10] L. Pawlowski, The Science and Engineering of Thermal Spray Coatings, John Wiley & Sons Ltd., London, 1995.